Papers on Anthropology XXXII/2, 2023, pp. 7–31

SPATIAL COMPLEXITY OF THE CEREBRAL CORTEX PIAL SURFACE: QUANTITATIVE ASSESSMENT BY TWO-DIMENSIONAL FRACTAL ANALYSIS OF MRI BRAIN SCANS

Nataliia Maryenko, Oleksandr Stepanenko

Department of Histology, Cytology and Embryology, Kharkiv National Medical University, Kharkiv, Ukraine

ABSTRACT

The objective of the current study was to evaluate the spatial complexity of the cerebral pial surface through two-dimensional fractal analysis of the external linear contour of cerebral hemispheres and to investigate the correlation between the parameters determined using Euclidean and fractal geometries.

Magnetic resonance brain images were obtained from 100 individuals (44 males and 56 females, aged 18–86 years). Five magnetic resonance images were selected from the MRI dataset of each brain, comprising four tomographic sections in the coronal plane and one section in the axial plane. Fractal dimension values of the linear contour of the pial surface of cerebral hemispheres were measured using the two-dimensional box counting method. Morphometric parameters based on Euclidean geometry were also determined (perimeter, area and their derivative values).

In this study, the obtained fractal dimension values were shown to be sensitive to the tortuosity of the linear contour of cerebral hemispheres, which depends on the number of gyri and sulci and the complexity of their shape. Therefore, the fractal dimension can be considered as an objective quantitative parameter characterizing the spatial complexity of the pial surface of cerebral hemispheres. The present study revealed that the Euclidean geometry-based morphometric parameters most strongly associated with the fractal dimension of the cerebral linear contour were the perimeter and the parameters calculated from perimeter values, including the perimeter-to-area ratio, shape factor, and two-dimensional gyrification index. Fractal dimension values did not exhibit strong correlations with age.

https://doi.org/10.12697/poa.2023.32.2.01

The data obtained in this study can be utilized for anatomical and anthropological studies. Furthermore, they hold practical applications in clinical contexts for diagnostic purposes, such as the diagnosis of congenital cerebral malformations and postnatal cerebral maldevelopment.

Keywords: *fractal analysis; fractal dimension; cerebral hemispheres; cerebral cortex; magnetic resonance imaging*

INTRODUCTION

Morphometric methods are widely employed in various studies involving the evaluation of the structural features of different organs and their components. The vast majority of morphometric methods used in classical anatomical and clinical structural studies are based on Euclidean geometry. Traditional morphometric methods provide sufficient information to characterize geometrically simple structures by determining their linear dimensions, area, volume, and various indices calculated from them.

However, there are anatomical structures with irregular geometric shapes that are challenging or impossible to characterize using traditional morphometric methods [11, 16]. Additionally, in some cases, it is advisable to assess the spatial configuration complexity of the structures under investigation. In these studies, fractal analysis becomes the most suitable and informative morphometric method. This mathematical analysis method is based on the principles of fractal geometry [20, 21]. Fractal analysis determines the fractal dimension (FD), which serves as a measure of the space-filling and spatial configuration complexity of the studied figures [1, 2, 11, 16, 20, 21].

Among the numerous anatomical structures and configurations found in the human body, the cerebrum stands out as one with the most intricate forms [1, 21]. Currently, classical morphometric studies are the most commonly used methods to quantify brain structures [6, 18, 25, 27, 30, 33]. Traditional morphometry encompasses volumetric studies, including measurements of grey and white matter volumes [6, 25, 27, 30, 33], assessment of cortical thickness [18, 25, 33], sulcal depth [18, 25], and the gyrification index [18, 33]. But the spatial configuration of the cerebral hemispheres, especially their pial surface, is too irregular for comprehensive assessment using traditional morphometric methods. The configuration of the cerebral surface and its complexity depends on the number of gyri and sulci as well as on the complexity of their shapes. The objectivity of assessing these parameters is particularly important for characterizing brain development in an individual's ontogenesis

and human phylogenesis as well as for diagnostic purposes in distinguishing between cerebral malformations or postnatal brain maldevelopment and the normal brain structure. It is challenging to comprehensively assess these parameters using a single metric, especially when applying methods derived from Euclidean geometry.

In recent decades, scientists have considered the cerebral cortex and its configuration a natural fractal [9, 14, 15]. Consequently, for a thorough examination of irregular structures like the cerebrum, various methods and adaptations of fractal analysis have been employed. In previous studies, various researchers have used fractal analysis to study the cerebral cortical ribbon [4, 7, 9, 13–15, 28], the pial surface of the cerebral cortex [7, 8, 10, 12, 13, 17, 19, 34], and the cerebral white matter [3, 5, 26, 31, 32], including its outer surface, which constitutes the linear boundary between the cortical ribbon and the white matter [5, 32]. However, despite the wealth of studies involving fractal analysis of brain structures, numerous questions persist, ranging from simplifying image pre-processing and analysis algorithms to adapting fractal analysis for diverse research types, including classical anatomical and anthropological studies [9]. In our previous works, we conducted fractal analysis of cerebral silhouettes [23] and linear contours [24] with the aim of assessing age-related changes in cerebral hemispheres. The objective of the current study extending on the previous ones [23, 24] was to evaluate the spatial complexity of the cerebral pial surface through two-dimensional fractal analysis of the external linear contour of cerebral hemispheres and to investigate the correlation between the parameters determined using fractal and Euclidean geometries.

MATERIALS AND METHODS

The present study was approved by the Commission on Ethics and Bioethics of Kharkiv National Medical University (minutes of the meeting of the Commission on Ethics and Bioethics of KhNMU No. 10 of November 7, 2018).

Subjects

In this research, magnetic resonance (MR) brain images were examined. The MR images were sourced from a cohort of 120 individuals. These participants had undergone MRI brain scanning at the Kharkiv Radiology Center for diagnostic purposes. The indications for MRI scanning varied among participants, with the most common reasons being headache, dizziness, and mild injuries to the soft tissues of the head. Additionally, some participants opted for

examination without specific complaints. The patients with severe neurological symptoms were not included in the study. The patients who expressed willingness to participate in the study provided signed informed consent. No financial or other interests were involved for the patients, the radiology experts, or the researchers. Written informed consent was obtained from all study participants before the MRI scanning took place.

The inclusion criterion for the study was age 18 and older, as we investigated the structural characteristics of the brain in adulthood. Patients who had not reached the age of majority (18 years) were not included in the study.

We excluded the MR images of 20 patients during the sample selection process for the following reasons: pathological changes in the brain or surrounding structures were identified; artifacts were detected in the scans (due to the presence of metallic dental prostheses, which caused interference in magnetic resonance imaging); MR images were taken with significant head tilt, and the projections differed from the standard; there were no coronal or axial sections (if tomography in any of these planes was not performed).

Therefore, only the MR images meeting stringent criteria, characterized by an absence of artifacts, adherence to the standard imaging protocol, and the absence of pathological findings, were included in our final sample comprising 100 subjects (44 males and 56 females). Their magnetic resonance imaging (MRI) data were categorized as relatively normal and were used for the study. Upon the selection of 100 MRI brain scans meeting these criteria, we concluded the selection process. We believe that this sample size is sufficient to yield statistically significant results for our study.

The final sample comprised individuals aged between 18 and 86 years. Among them, 31 persons were between 18 and 30 years old, 29 persons between 31 and 45 years, 24 persons between 46 and 60 years, and 16 persons between 61 and 86 years. Their average age was 41.72 ± 1.78 years.

MRI protocol

MRI brain scans were obtained using a 1.5 Tesla MRI machine (Siemens Magnetom Symphony). During the preparation for scanning, patients' heads were fixed to prevent head tilting and involuntary movements during scanning; the head position during fixation was standardized. Since the brain tomography of all patients was conducted using the same magnetic resonance scanner with an identical protocol, we consider the MR brain sections (and the planes in which the tomography was performed) of different patients to be comparable.

The study employed T2 and FLAIR sequences, with the following MRI parameters: for the T2 sequence: Echo Time (TE): 130 ms; Repetition Time (TR): 4440 ms; for the FLAIR sequence: Echo Time (TE): 114 ms; Repetition Time (TR): 9000 ms; Inversion Time (TI): 2500 ms. In both MRI sequences, the slice (section) thickness was 5 mm. The digital MR brain images had a resolution of 72 pixels per inch, and the absolute image scale was 3 pixels per 1 mm.

Selection of tomographic sections

A total of 500 MR brain images from 100 subjects were selected for analysis. Five MR images were chosen from the MRI dataset of each individual. These five images comprised four tomographic sections in the coronal (frontal) plane and one section in the axial (horizontal) plane. The selection of image sets adhered to specific criteria:

- Location: the images were taken from different areas of the cerebral hemispheres;
- Identifiability: they were chosen for easy identification based on anatomical landmarks;
- Pathological relevance: the images included brain regions where pathological lesions are commonly observed in certain neurodegenerative diseases, such as Alzheimer's disease [14].

The tomographic sections were defined as follows:

1. Coronal 1: located at the level of the anterior points of the temporal lobes;
2. Coronal 2: level of the mamillary bodies (corpus mamillare);
3. Coronal 3: level of the quadrigeminal plate (lamina quadrigemina);
4. Coronal 4: level of the posterior pole of the corpus callosum (splenium corpori callosi);
5. Axial: level of the thalamus.

Image pre-processing

In the image processing workflow, blank frame images were generated using the Adobe Photoshop CS5 graphics editor. Digital fragments from the MR images were then integrated into these blank frame images. Image scaling was not employed at this processing stage; all pixels of the original image were copied and pasted into a frame image as they are. The tomographic sections of the cerebral hemispheres were completely placed within the frames without extending beyond them, as illustrated in Fig. 1, A. The dimensions of the frame

images for coronal sections were set at 512 × 400 pixels, while for axial sections, they were 512 × 800 pixels. These dimensions were determined to ensure that all copied fragments of MR images (even with the largest head size) fit completely into this frame.

To ensure precise segmentation of the cerebral hemispheres' sections, structures surrounding these sections were initially removed from the images (Fig. 1, B). The respective image areas were manually selected and filled with white pixels (with a pixel intensity value of 255) for T2 sequence or black pixels (with a pixel intensity value of 0) for FLAIR sequence using the graphic editor.

Preliminary, or "rough", segmentation was achieved through image thresholding, with a pixel intensity threshold value of 128 for T2 sequence and 65 for FLAIR sequence. The thresholding values were determined empirically. Initially, various thresholding values were applied for MR brain images of 10 individuals, and we visually compared the results with the non-segmented MR images. The thresholding values that provided satisfactory results across all studied samples were selected for further image processing. The thresholding process converted the grayscale MR images into a binary format.

Subsequently, a more accurate segmentation was carried out to enhance the anatomical fidelity of the resulting silhouette brain images, as illustrated in Fig. 1, C. This step involved manual corrections using Adobe Photoshop CS5 tools. Manual correction was performed by two researchers. Initially, the first researcher carried out manual correction on all images and then provided the corrected images to the second researcher. The second researcher conducted validation and, if necessary, corrected the images, returning them to the first researcher for agreement on the changes made. Thus, all images underwent the same manual correction and validation algorithm, ensuring that the parameters of the entire sample were comparable.

The silhouette brain images were outlined with a line thickness of 1 pixel, and from this, linear contours of the cerebral pial surface were derived, as shown in Figure 1, D. This preprocessing procedure was applied to all the 500 selected images (Figure 2).

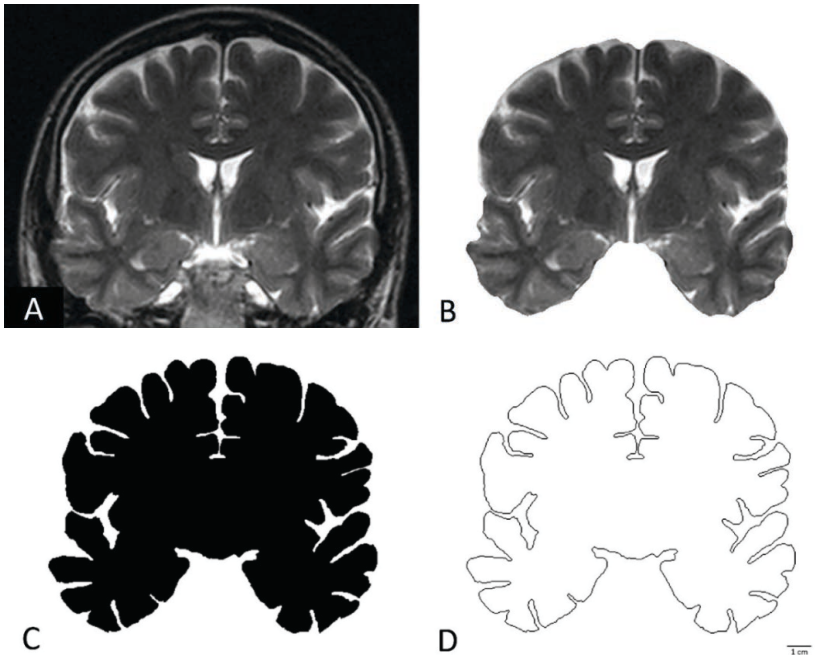

Figure 1. Pre-processing of MR brain images. A – MR image of cerebral hemispheres (Coronal 2, level of mammillary bodies); B – non-segmented tomographic section after background removal; C – segmented silhouette image; D – outlined image displaying the outer linear contour of cerebral hemispheres' pial surface. Scale bar = 1 cm.

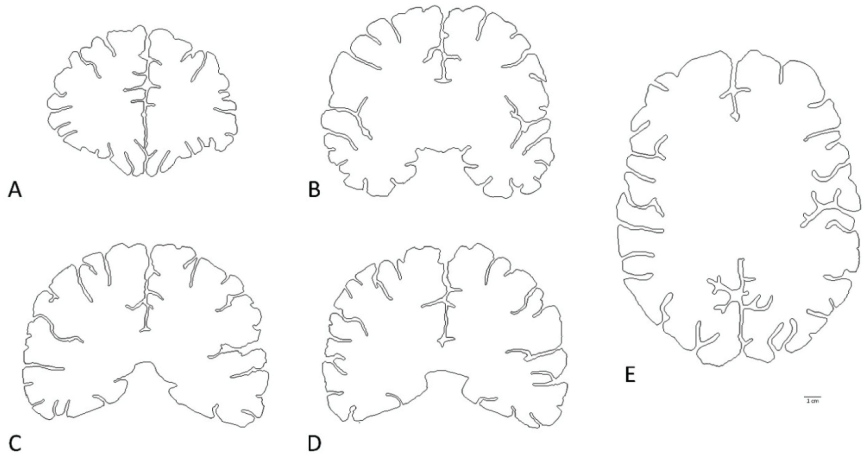

Figure 2. Linear contours of cerebral hemispheres revealed after preprocessing of MR images of different localizations. A – Coronal 1, level of temporal lobes anterior pole, B – Coronal 2, level of mammillary bodies, C – Coronal 3, level of quadrigeminal plate, D – Coronal 4, level of corpus callosum posterior pole, E – Axial, thalamus level. Scale bar = 1 cm.

Fractal analysis

The fractal analysis was conducted using the two-dimensional box counting method, which is considered the "gold standard" among fractal analysis methods due to its simplicity and universality [11].

During fractal analysis, a grid is overlaid on the image, dividing it into boxes (squares) of a specified size (box size). The analysis is performed in several sequential iterative stages, each with a changing box size. In our study, nine stages of fractal analysis were employed with the following box size values: 64, 32, 16, 12, 8, 6, 4, 3, and 2 pixels (Fig. 3, Table 1).

At each stage of fractal analysis, the number of boxes (N) intercepting a fragment of the investigated object (in our work – the outlined contour of the cerebral hemispheres) is calculated, ignoring "empty" boxes. Figure 3 explains the algorithm of fractal analysis used in the present study. The fragments from Figure 2, A (section Coronal 1), sized 192 × 192 pixels and 72 × 72 pixels, were used for illustrative clarity to demonstrate box counting at convenient magnifications. However, fractal analysis was conducted for the entire images, which were sized 512 × 400 pixels and 512 × 800 pixels for coronal and axial sections, respectively.

The count of "filled" boxes can be done manually or automatically. In our work, we utilized automated counting with the "Fractal box count" tool in the Image J software [29].

For calculating the FD value (Table 1), the reciprocal value of box size (1 / box size) is computed, and its natural logarithm is determined (LN (1 / box size)). The natural logarithm of N (LN(N)) is also calculated.

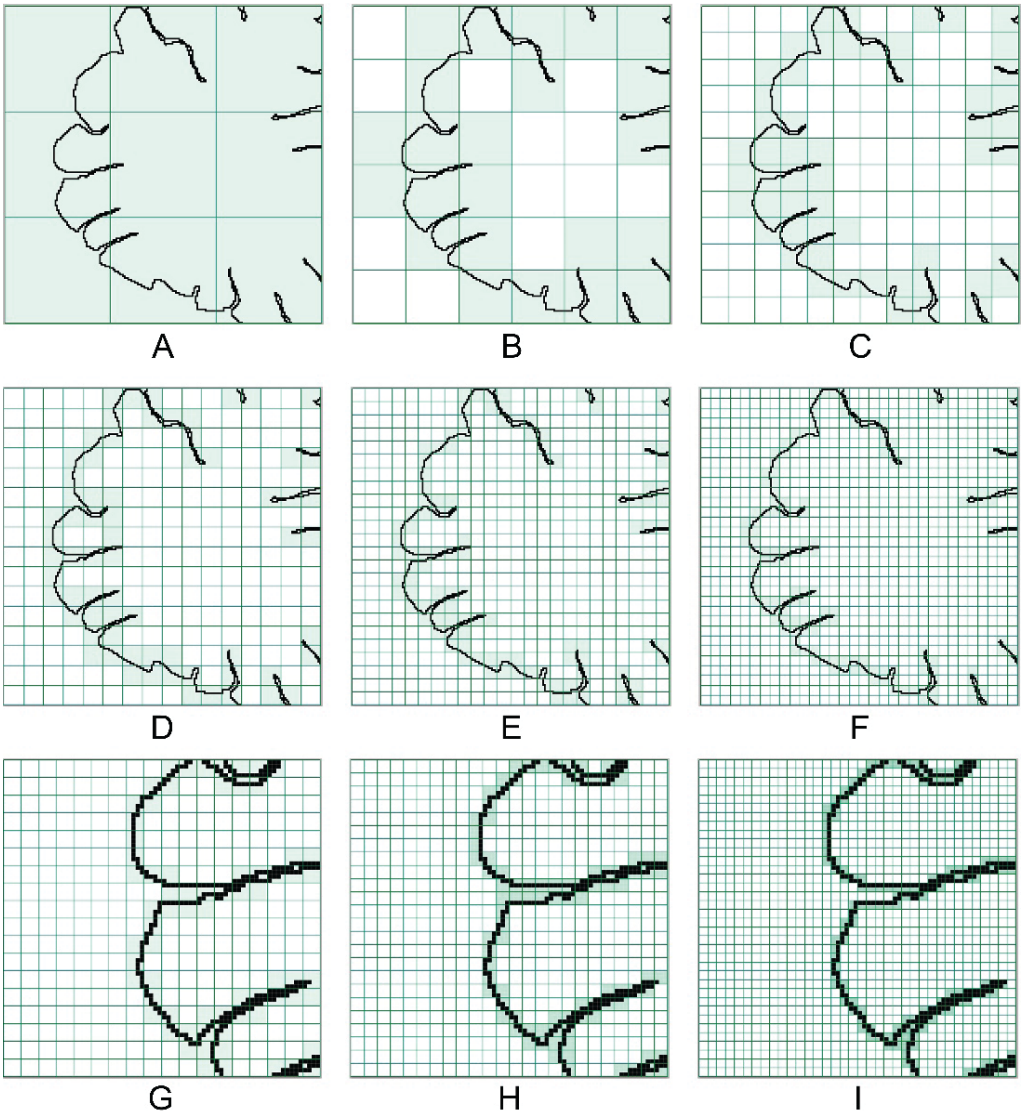

Figure 3. The principle of the fractal analysis using the two-dimensional box counting method. The illustration shows fragments from Figure 2A (section Coronal 1). The size of the fragments is as follows: A–F – 192 × 192 pixels; G–I – 72 × 72 pixels. A – 1st stage of fractal analysis, box size – 64 pixels; B – 2nd stage, box size – 32 pixels; C – 3rd stage, box size – 16 pixels; D – 4th stage, box size – 12 pixels; E – 5th stage, box size – 8 pixels; F – 6th stage, box size – 6 pixels; G – 7th stage, box size – 4 pixels; H – 8th stage, box size – 3 pixels; I – 9th stage, box size – 2 pixels. Boxes intercepting the studied object (outlined contour of cerebral hemispheres) are highlighted with a darker background.

Table 1. Data used for fractal analysis using the two-dimensional box counting method.

Parameter	Stage of fractal analysis								
	1	2	3	4	5	6	7	8	9
Box size (pixels)	64	32	16	12	8	6	4	3	2
1/Box size	0.016	0.031	0.063	0.083	0.125	0.167	0.250	0.333	0.500
LN(1/Box size)	*–4.159*	*–3.466*	*–2.773*	*–2.485*	*–2.079*	*–1.792*	*–1.386*	*–1.099*	*–0.693*
N	20	62	160	226	379	522	840	1173	1834
LN(1/N)	*2.996*	*4.127*	*5.075*	*5.421*	*5.938*	*6.258*	*6.733*	*7.067*	*7.514*

Subsequently, the linear regression equation $y = b \times x + a$ is computed, where LN (1 / Box size) is the independent variable x, and LN(N) is the dependent variable y. The FD corresponds to coefficient b, which represents the estimated slope of the regression line, and coefficient a is the estimated intercept (Fig. 4). Thus, based on the example calculations (Table 1), FD was determined to be 1.2837 (Fig. 4).

The calculation of FD values in our study was done using the "Fractal box count" tool in the Image J software.

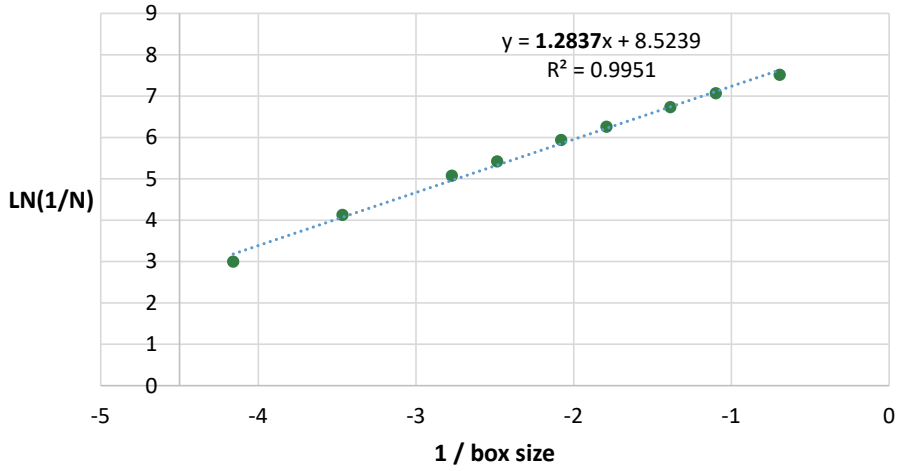

Figure 4. Fractal analysis using the two-dimensional box counting method. Calculation of the fractal dimension (FD) value. FD corresponds to the coefficient representing the estimated slope of the regression line. In this example, the FD value equals 1.2837

The described procedure of fractal analysis was performed individually for each of the 500 pre-processed outlined images. The fractal analysis yielded FD values in five distinct sections for each subject. Additionally, we computed the average

FD value of all five sections as well as the average FD value derived from the four coronal sections.

Euclidean geometry-based image morphometry

We calculated morphometric parameters based on Euclidean geometry (the detailed analysis of these parameters was done in our previous study [22]), including perimeter (P), area (A), perimeter-to-area ratio (P/A), and shape factor (SF). The shape factor (SF) was determined using the formula: $SF = (4\pi \times A) / P^2$. These parameters were calculated based on two types of images.

The first type of images included non-segmented tomographic sections (Fig. 1, B). In these images, the perimeter corresponds to the contour of the superficially exposed surface of cerebral hemispheres, and the area includes the brain tissue as a whole, encompassing the contents of the sulci. The following parameters were determined for these images: P_0 (perimeter), A_0 (area), P_0 / A_0 (perimeter-to-area ratio), and SF_0 (shape factor).

The second type of images included segmented silhouette images (Fig. 1, C). In these images, the perimeter corresponds to the contour of the entire pial surface of the cerebral hemispheres, including the pial surface contour within the sulci, and the area includes the brain tissue as a whole but excludes the contents of the sulci. The following parameters were determined for these images: P_S (perimeter), A_S (area), P_S / A_S (perimeter-to-area ratio), and SF_S (shape factor).

Additionally, we calculated the ratios of the perimeter and the area of segmented silhouette images to the corresponding parameters of non-segmented images (P_S / P_0 and A_S / A_0, respectively). The ratio of the two perimeters (P_S / P_0) can be considered a two-dimensional equivalent of the gyrification index since it characterizes the ratio of the length of the entire pial surface contour of the cerebral hemispheres to the length of the superficially exposed surface contour (the original gyrification index is determined as the ratio of the total area of the pial surface of cerebral cortex to the area of superficially exposed cerebral surface).

Statistical data processing

Statistical data processing was performed using Excel 2016 software. The following values were calculated: the median (Me, or the 50th percentile value), the values of the 25th and 75th percentiles, and the minimum (min) and maximum (max) values.

The normality of the distribution was assessed using the Shapiro-Wilk W test. The significance of statistical differences between the FD values measured in different tomographic sections was evaluated using the Kruskal-Wallis H test, followed by post-hoc Dunn's test with Bonferroni adjustment for multiple comparisons.

To characterize the correlation relationships, Spearman's rank correlation coefficient (r) was computed, and the significance of these correlations was tested using Student's T test. The significance level of $p < 0.05$ was applied to all results.

RESULTS

The statistical descriptive parameters of the FD values obtained in this study are presented in Figure 5. The normality of the FD value distributions was assessed, and the results showed that the distributions of FD values for sections Coronal 1 ($p = 0.466$), Coronal 2 ($p = 0.618$), Coronal 4 ($p = 0.131$), and Axial ($p = 0.779$) did not significantly deviate from a normal distribution. However, the distribution of FD values for section Coronal 3 was found to be skewed and significantly differed from a normal distribution ($p = 0.012$). This skewness can be attributed to anatomical variations in this specific brain region, as well as the heterogeneity of the data and the limited sample size. The distributions of the average FD values for all five sections and the average FD values for the four coronal sections were also not significantly different from a normal distribution ($p = 0.380$ and $p = 0.360$, respectively).

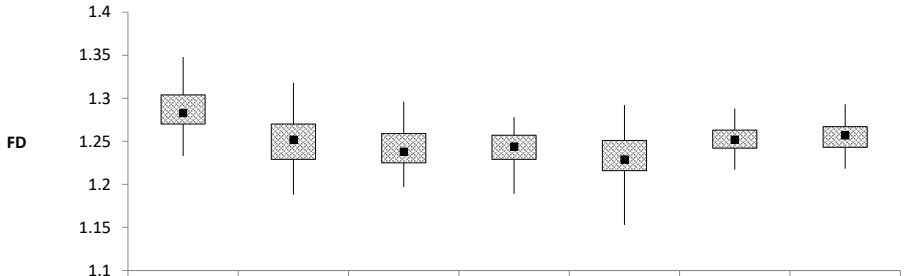

	Coronal 1	Coronal 2	Coronal 3	Coronal 4	Axial	Average all sections)	Average (1-4 coronal)
percentile 75	1.304	1.27	1.259	1.257	1.251	1.263	1.267
Max	1.348	1.318	1.296	1.278	1.292	1.288	1.293
■ Me	1.283	1.252	1.238	1.244	1.229	1.252	1.257
Min	1.233	1.188	1.197	1.189	1.153	1.217	1.218
percentile 25	1.27	1.229	1.225	1.229	1.216	1.242	1.243

Figure 5. Statistical parameters of FD values of cerebral hemispheres' linear contour.

The FD values of the linear contour of the cerebral hemispheres exhibited low coefficients of variation (ranging from 1.28% to 2.37%), indicating minimal variability in the FD values. Figure 6 illustrates two linear contours of the cerebral hemispheres with the minimum and maximum FD values (1.197 and 1.296, respectively) for a specific tomographic section (in this case, Coronal 3 sections are shown as an example). It is evident that the contour with the maximum FD value displayed a greater number of gyri and sulci as well as a more intricate configuration compared to the contour with the minimum FD value. This observation emphasizes that even a modest increase by approximately 0.1 in the FD value corresponds to a notable enhancement in the complexity of the spatial configuration of the linear contour. Thus, despite its low variability, FD demonstrated its sensitivity and informativeness as a morphometric parameter.

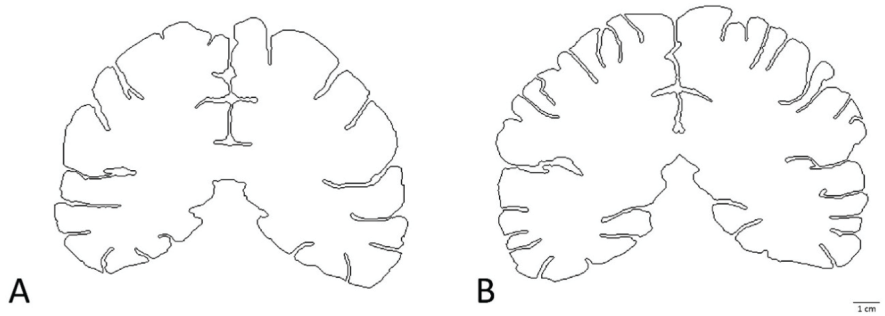

Figure 6. Linear contours of cerebral hemispheres (Coronal 3, level of quadrigeminal plate) with a low FD value (A, FD = 1.197) and a high FD value (B, FD = 1.296). Scale bar = 1 cm.

Comparisons of FD values among the five tomographic sections revealed that the lowest FD values were observed in the Axial section, while the highest FD values were found in section Coronal 1. The Kruskal-Wallis H test indicated a significant difference in FD values among the five sections ($\alpha = 0.05$, $p \approx 0$). Since the p-value < α, the null hypothesis was rejected. Subsequent post-hoc Dunn's tests, using a Bonferroni-corrected α of 0.005, revealed that the mean ranks of FD values significantly differed between the following section pairs: Coronal 1 – Coronal 2, Coronal 1 – Coronal 3, Coronal 1 – Coronal 4, Coronal 1 – Axial, and Coronal 2 – Axial ($p < 0.001$). Additionally, the tests indicated that the mean ranks of FD values did not significantly differ between the following section pairs: Coronal 2 – Coronal 3 ($p = 0.023$), Coronal 2 – Coronal 4 ($p = 0.020$), Coronal 3 – Coronal 4 ($p = 0.956$), Coronal 3 – Axial ($p = 0.044$), and Coronal 4 – Axial ($p = 0.050$).

Correlation analysis was conducted to identify and describe the correlation relationships between FD values of the five tomographic sections (Table 2, Fig. 7). The adjacent coronal sections showed the closest relationships. Significant positive correlations were observed between the FD values of the following section pairs: Coronal 1 – Coronal 2, Coronal 2 – Coronal 3, Coronal 3 – Coronal 4, Coronal 1 – Coronal 3, Coronal 2 – Coronal 4, and Axial – Coronal 3. No statistically significant correlations were found between the FD values of all other tomographic sections.

Table 2. Correlation coefficients (r) characterizing relationships of the FD values of cerebral hemispheres' linear contours measured in different tomographic sections.

Tomographic section of cerebral hemispheres	Coronal 1	Coronal 2	Coronal 3	Coronal 4	Axial
Coronal 1	–	0.242*	0.290**	0.122	–0.055
Coronal 2	0.242*	–	0.443***	0.443***	0.103
Coronal 3	0.290**	0.443***	–	0.509***	0.299**
Coronal 4	0.122	0.443***	0.509***	–	0.176
Axial	–0.055	0.103	0.299**	0.176	–

Statistical significance of correlation coefficient (r): * – $p < 0.05$, ** – $p < 0.01$, *** – $p < 0.001$.

Correlation relationships between FD values and morphometric parameters of non-segmented tomographic sections were analysed (Table 3, Fig. 8). Significant correlations were observed only between the parameters of sections Coronal 1 and Coronal 2. Negative correlations were found between FD values and the values of perimeter (P_0), area (A_0), and shape factor (SF_0), while a positive correlation was found between FD values and the perimeter-to-area ratio (P_0 / A_0).

Additionally, correlation relationships between FD values and morphometric parameters of segmented silhouette images were examined (Table 3). Significant correlations were observed between FD values and most morphometric parameters. Positive correlations were noted between the FD values of all sections and the perimeter values (P_S) as well as between the FD values and the perimeter-to-area ratio (P_S / A_S). However, significant negative correlations were found between the FD values and area values (A_S) only in section Coronal 1. Significant negative correlations were observed between the FD values and the values of the shape factor (SF_S) in all five tomographic sections.

There were also significant positive correlations between the FD values and the values of the two-dimensional gyrification index (P_S / P_0) in all localizations. However, the ratio of the areas of the two studied image types (A_S / A_0) exhibited significant negative correlations with FD of Coronal 3 and Axial sections.

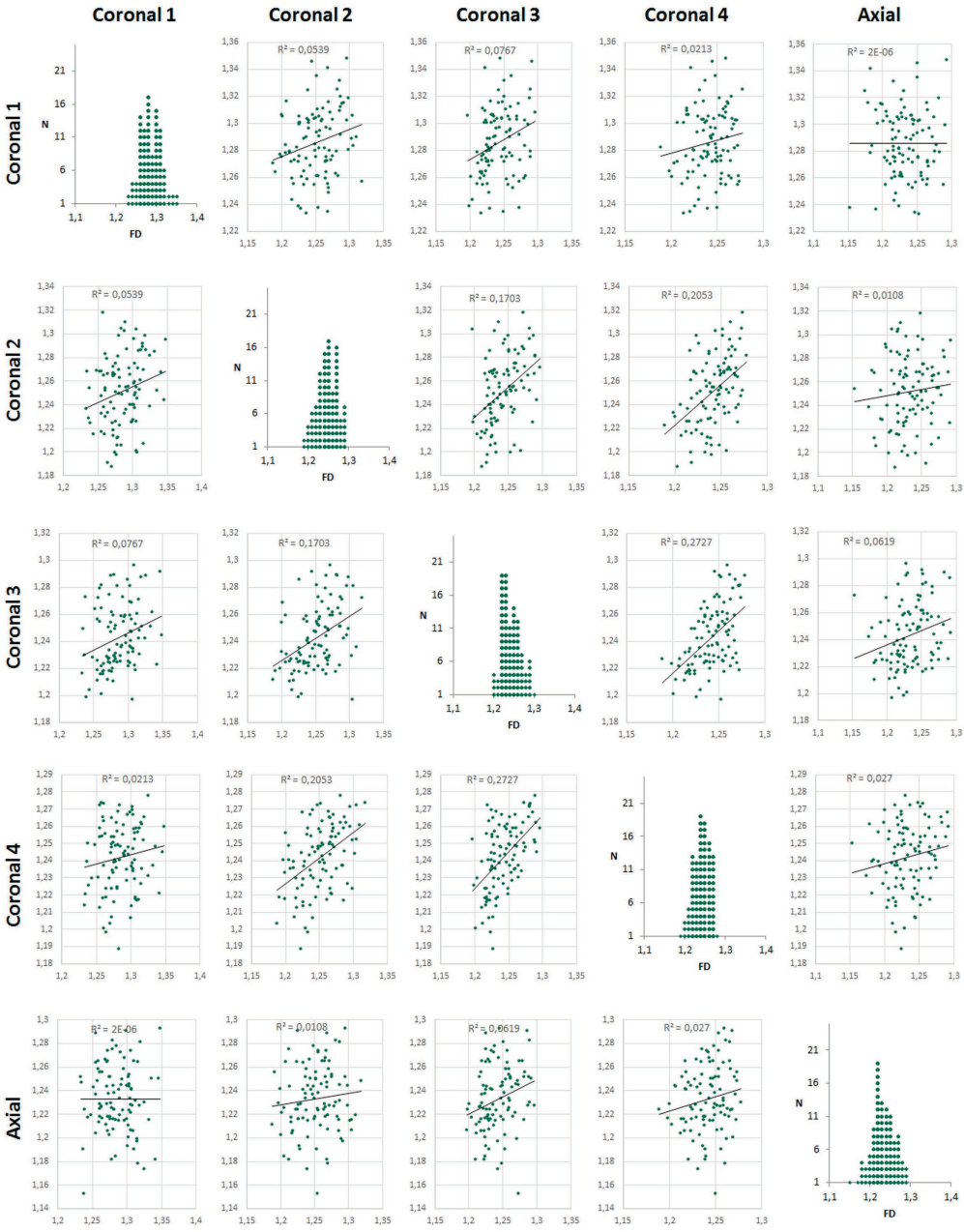

Figure 7. Correlation matrix characterizing relationships of the FD values of cerebral hemispheres' linear contours measured in different tomographic sections.

Table 3. Correlation coefficients (r) characterizing relationships of the FD values and Euclidean geometry-based morphometric parameters of cerebral hemispheres.

Type of images	Morphometric parameter		Tomographic section of cerebral hemispheres				
			Coronal 1	Coronal 2	Coronal 3	Coronal 4	Axial
Non-segmented tomographic sections	P_0	Perimeter	–0.246*	–0.200*	0.127	–0.023	0.087
	A_0	Area	–0.349***	–0.159	0.065	–0.021	0.112
	P_0/A_0	Perimeter-to-area ratio	0.353***	0.078	0.013	0.043	–0.036
	SF_0	Shape Factor	–0.197	0.091	–0.080	0.016	0.059
Segmented silhouette images	P_s	Perimeter	0.176	0.467***	0.558***	0.507***	0.572***
	A_s	Area	–0.350***	–0.133	–0.021	–0.007	–0.048
	P_s/A_s	Perimeter-to-area ratio	0.553***	0.537***	0.541***	0.463***	0.530***
	SF_s	Shape Factor	–0.478***	–0.566***	–0.604***	–0.552***	–0.592***
Both types of images	P_s/P_0	Ratio of perimeters (2D gyrification index)	0.378***	0.641***	0.609***	0.642***	0.560***
	A_s/A_0	Ratio of areas	–0.175	–0.094	–0.223*	0.005	–0.441***

Statistical significance of correlation coefficient (r): * – $p < 0.05$, ** – $p < 0.01$, *** – $p < 0.001$.

The study determined the values of the correlation coefficient between the FD values and age (Table 4, Fig. 9). Significant correlations were found between age and FD values of sections Coronal 2 and Coronal 4 as well as between age and the average FD value of four coronal sections. However, no significant correlations were found between age and the FD values of all other tomographic sections. Taking into account the slight decrease of some FD values during adulthood, we calculated 95% confidence intervals of FD values (Fig. 9) which can serve as normative criteria for similar studies.

Table 4. Correlation coefficients (r) characterizing relationships of the FD values of cerebral hemispheres and age.

r	Tomographic section of cerebral hemispheres						
	Coronal 1	Coronal 2	Coronal 3	Coronal 4	Axial	Average (all sections)	Average (1–4 coronal)
Age, years	–0.032	–0.206*	–0.128	–0.253*	0.196	–0.143	–0.243*

Statistical significance of correlation coefficient (r): * – $p < 0.05$.

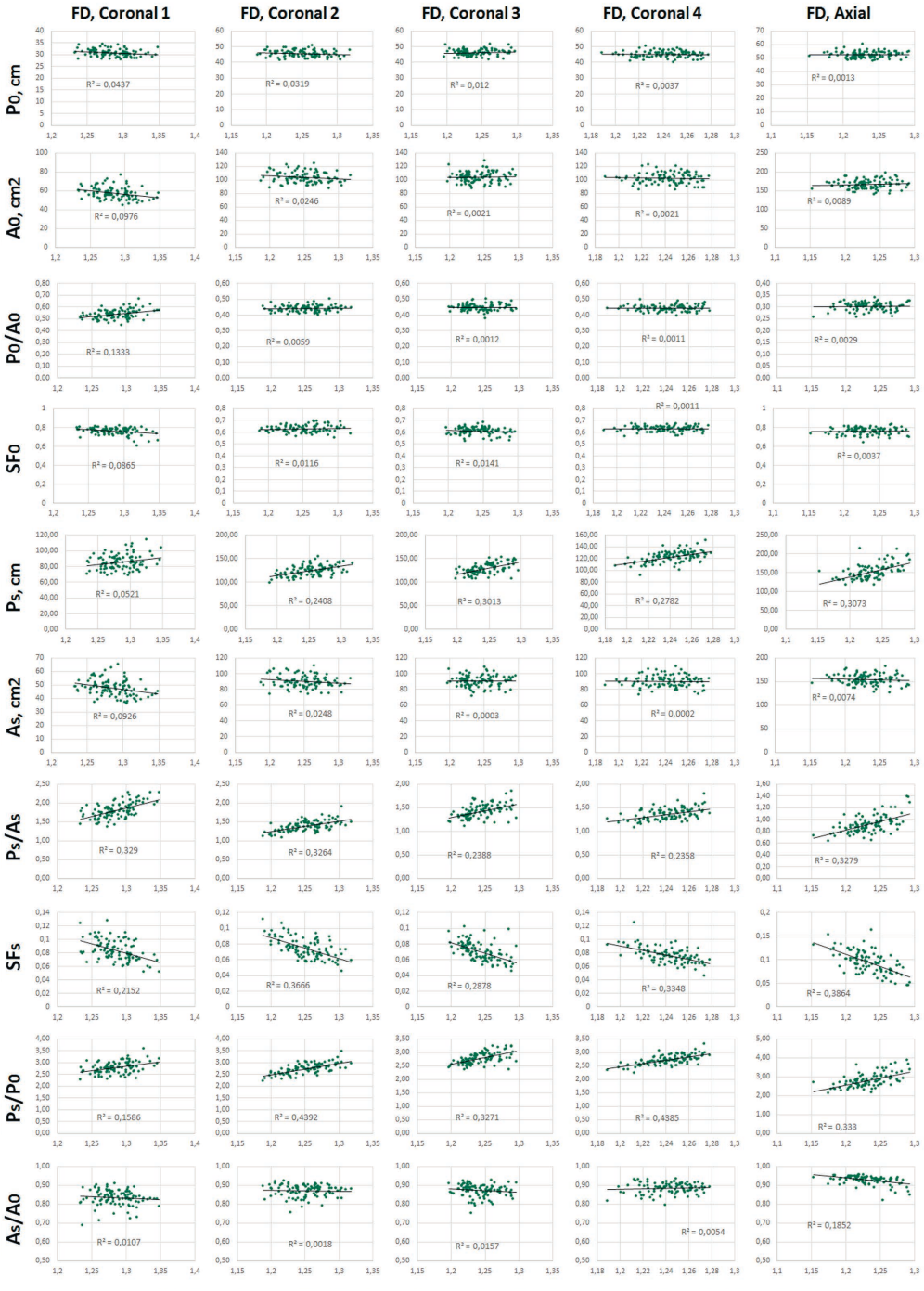

Figure 8. Correlation matrix characterizing relationships of the FD values and Euclidean geometry-based morphometric parameters of cerebral hemispheres.

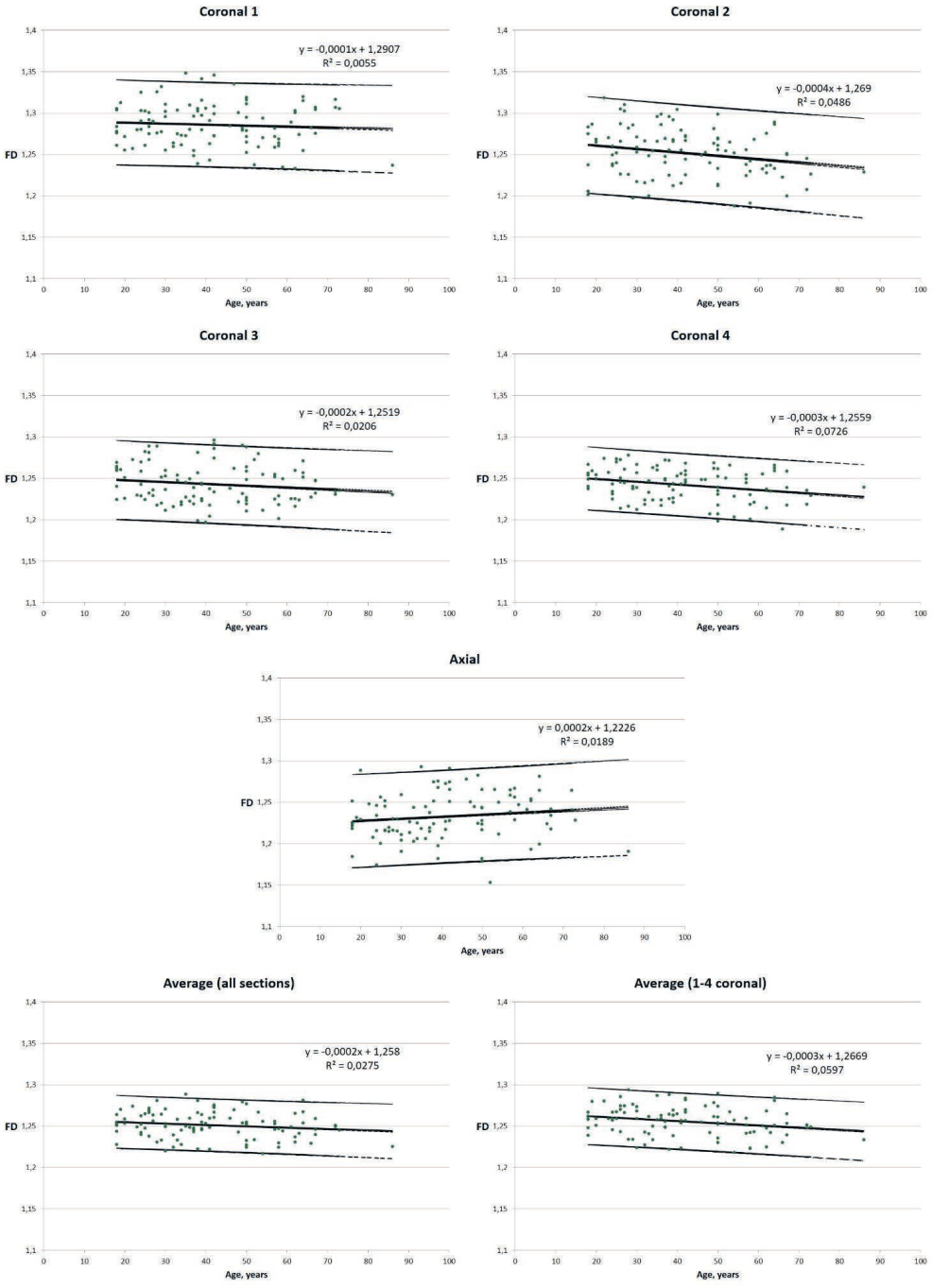

Figure 9. Distribution of FD values throughout adulthood and 95% confidence intervals for the FD values of cerebral hemispheres' linear contours.

DISCUSSION

In this study, we described the features of cerebral hemispheres' spatial configuration using the methods of both fractal geometry and Euclidean geometry. As the object of study, we chose the cerebral hemispheres' pial surface, the FD of which allowed us to estimate cerebral spatial complexity. The FD values obtained in this study proved particularly sensitive to the overall complexity of the linear cerebral contour, which is contingent on the number of gyri and sulci. This assertion is supported by the fact that FD values exhibited the strongest correlations with morphometric parameters based on Euclidean geometry indirectly reflecting the tortuosity of the linear contour. These parameters include perimeter (representing the length of the contour under investigation) and parameters derived from perimeter values, such as the perimeter-to-area ratio, shape factor, and the two-dimensional gyrification index. Given that the numbers of gyri and sulci are inherent features, the FD values determined in this study serve as a quantifiable means of characterizing the individual anatomical features of the cerebral hemispheres. These findings align with those of other researchers who have reported positive correlations between FD and the gyrification index as well as significant associations between FD and volumes of grey and white matter, and cortical thickness [8, 10, 19]. However, the FD values almost did not correlate with the area values of the images. This finding supports the fact that the FD of the contours is independent of the size and scale of the image.

The present study utilized two-dimensional approach of fractal analysis; thus, several FD values were determined for each brain. The Axial section exhibited the lowest FD values, while the highest FD values were found in Coronal section 1. In our opinion, the FD values of different brain sections are expected to differ since the configuration of different brain areas varies, reflecting anatomical features. By examining and comparing the contours of different tomographic sections in Figure 2, we can observe that the gyri and sulci contours of section Coronal 1 are denser, leaving less free space inside, which accounts for the highest FD values. In contrast, the contour of the Axial section fills less space, resulting in relatively lower FD values. However, expecting identical FD values and high correlation coefficients between them would be justified if the brain had a simplified shape (similar to a cylinder) with gyri and sulci running along the axis of the cylinder. In that case, the configuration of contours would be similar across different sections since the same gyri and sulci would be captured in each section. However, the shape of the brain is more complex, so the configuration of the pial surface differs in different brain sections.

Previous studies concerning the cerebral surface have predominantly employed the three-dimensional version of fractal analysis [7, 8, 10, 13, 17, 19, 34], while two-dimensional studies have been significantly fewer [12]. The three-dimensional version of fractal analysis undoubtedly offers advantages as it provides an estimation of the entire shape of the cerebral hemispheres [7, 8, 10, 13, 17, 19, 34]. Nevertheless, most three-dimensional adaptations necessitate the construction of three-dimensional brain models, which can be challenging or impossible in certain scenarios (such as when working with overly thick tomographic sections, low-quality images, or anatomical specimens [9]). In such situations, two-dimensional analysis can serve as a viable alternative. Moreover, two-dimensional analysis is practical when a quick assessment of a two-dimensional image is needed, either as an independent study or as a preliminary investigation to determine the necessity of conducting a three-dimensional study. While the FD determined on three-dimensional images characterizes the surface of cerebral hemispheres as a whole, the FD determined on two-dimensional images characterizes only a specific area of the brain. This particularity of two-dimensional analysis serves as both its limitation and its advantage. Therefore, this research method is suitable for situations where it is essential to assess only a specific region of the brain, such as a particular tomographic section. In our opinion, in such cases, opting for a two-dimensional version of fractal analysis is advisable.

The study most closely related to ours is the work of E. Kalmanti and T. G. Maris [12], which provided a fractal analysis of the cerebral cortex linear contours in a two-dimensional variant. However, this study differed from our present study in methodological approaches. Firstly, during preprocessing, the authors identified cortical areas and outlined them, thus studying inner and outer cortical contours simultaneously (including the contour of the pial surface and the boundary between the cortex and white matter), while we studied the contours of the pial surface. Secondly, the authors focused on parasagittal sections, while we utilized coronal and axial sections. We chose coronal and axial planes for our study because we believe that these sections should cut across the gyri and sulci, thereby revealing their contours. In this context, coronal and axial planes are more suitable for such studies.

Another two-dimensional study of cerebral MR images, partially similar to the present one, is by R. D. King et al. [14], in which a fractal analysis of two-dimensional MR brain images was also conducted. The authors used similar MR planes and sections and provided a fractal analysis of cortical ribbons, while our study determined the FD values of the linear contours. The authors re-

ported a significant decrease in cortical FD in patients with Alzheimer's disease compared to healthy individuals.

In our previous studies, we examined the same sample using alternative two-dimensional fractal analysis algorithms that have proven to be sensitive to age-related atrophic changes in cerebral hemispheres: fractal analysis of silhouette images using the box counting method [23] and fractal analysis of cerebral contours using the novel contour smoothing method [24]. In several prior investigations conducted by other researchers, FD values exhibited strong and significant negative correlations with age [5, 7, 19, 25, 31]. However, in the current study, FD values for the linear contour of the cerebral hemispheres, as determined by using the box counting method, did not show strong correlations with age. This observation can be attributed to the distinct sensitivities of various techniques, each capturing different aspects and changes in brain structure, including individual anatomical variations, atrophic alterations associated with normal aging, and pathological changes resulting from various conditions. The FD values obtained in the present study primarily depend on cerebral anatomical characteristics: the number of gyri and sulci as well as the features of their shape. These features arise from brain development during embryogenesis and the postnatal period, characterizing brain development in human phylogenesis as well. However, they do not significantly change during adulthood, explaining the relatively low sensitivity of the methodology used to age-related atrophic changes.

The present study faced several limitations. The study involved a sample size of 100 participants, and while efforts were made to include a diverse range of individuals, the findings may not be fully representative of the entire population. The participants were recruited from among individuals undergoing MRI for various clinical reasons, potentially introducing a bias towards individuals with specific health concerns. This may limit the generalizability of the results to healthier populations. The study focused on two-dimensional fractal analysis utilizing a limited number of sections (4 coronal and 1 axial), which, while informative for specific brain regions, may not capture the full complexity of three-dimensional structures.

The data obtained in this study can be utilized for anatomical and anthropological studies, regardless of the source materials employed, whether they are MRI, CT brain images or cadaveric specimens. Furthermore, they hold practical applications in clinical contexts for diagnostic purposes, such as the diagnosis of congenital cerebral malformations and postnatal cerebral maldevelopment.

REFERENCES

1. Di Ieva A., Esteban F. J., Grizzi F., Klonowski W., Martín-Landrove M. (2015). Fractals in the neurosciences, Part II: clinical applications and future perspectives. The Neuroscientist, 21(1), 30–43. https://doi.org/10.1177/1073858413513928
2. Di Ieva A., Grizzi F., Jelinek H., Pellionisz A. J., Losa G. A. (2014). Fractals in the Neurosciences, Part I: General Principles and Basic Neurosciences. The Neuroscientist, 20(4), 403–417. https://doi.org/10.1177/1073858413513927
3. Esteban F. J., Sepulcre J., de Mendizábal N. V., Goñi J., Navas J., de Miras J. R., Bejarano B., Masdeu J. C., Villoslada, P. (2007). Fractal dimension and white matter changes in multiple sclerosis. NeuroImage, 36(3), 543–549. https://doi.org/10.1016/j.neuroimage.2007.03.057
4. Esteban F. J., Sepulcre J., de Miras J. R., Navas J., de Mendizábal N. V., Goñi J., Quesada J. M., Bejarano B., Villoslada, P. (2009). Fractal dimension analysis of grey matter in multiple sclerosis. Journal of the Neurological Sciences, 282(1–2), 67–71. https://doi.org/10.1016/j.jns.2008.12.023
5. Farahibozorg S., Hashemi-Golpayegani S. M., Ashburner J. (2015). Age- and sex-related variations in the brain white matter fractal dimension throughout adulthood: an MRI study. Clinical Neuroradiology, 25(1), 19–32. https://doi.org/10.1007/s00062-013-0273-3
6. Ge Y., Grossman R. I., Babb J. S., Rabin M. L., Mannon L. J., Kolson D. L. (2002). Age-related total gray matter and white matter changes in normal adult brain. Part I: volumetric MR imaging analysis. AJNR American Journal of Neuroradiology, 23(8), 1327–1333.
7. Goñi J., Sporns O., Cheng H., Aznárez-Sanado M., Wang Y., Josa S., Arrondo G., Mathews V. P., Hummer T. A., Kronenberger W. G., Avena-Koenigsberger A., Saykin A. J., Pastor M. A. (2013). Robust estimation of fractal measures for characterizing the structural complexity of the human brain: optimization and reproducibility. NeuroImage, 83, 646–657. https://doi.org/10.1016/j.neuroimage.2013
8. Ha T. H., Yoon U., Lee K. J., Shin Y. W., Lee J. M., Kim I. Y., Ha K. S., Kim S. I., Kwon J. S. (2005). Fractal dimension of cerebral cortical surface in schizophrenia and obsessive-compulsive disorder. Neuroscience Letters, 384(1–2), 172–176. https://doi.org/10.1016/j.neulet.2005.04.078
9. Hofman M. A. (1991). The fractal geometry of convoluted brains. Journal of Hirnforschung, 32(1), 103–111.
10. Im K., Lee J. M., Yoon U., Shin Y. W., Hong S. B., Kim I. Y., Kwon J. S., Kim S. I. (2006). Fractal dimension in human cortical surface: multiple regression analysis with cortical thickness, sulcal depth, and folding area. Human Brain Mapping, 27(12), 994–1003. https://doi.org/10.1002/hbm.20238

11. Jelinek H. F., Fernandez E. (1998). Neurons and fractals: how reliable and useful are calculations of fractal dimensions? Journal of Neuroscience Methods, 81 (1–2), 9–18. https://doi.org/10.1016/s0165-0270(98)00021-1
12. Kalmanti E., Maris T. G. (2007). Fractal dimension as an index of brain cortical changes throughout life. In Vivo, 21(4), 641–646.
13. King R. D., Brown B., Hwang M., Jeon T., George A. T., Alzheimer's Disease Neuroimaging Initiative (2010). Fractal dimension analysis of the cortical ribbon in mild Alzheimer's disease. NeuroImage, 53(2), 471–479. https://doi.org/10.1016/j.neuroimage.2010.06.050
14. King R. D., George A. T., Jeon T., Hynan L. S., Youn T. S., Kennedy D. N., Dickerson B., Alzheimer's Disease Neuroimaging Initiative (2009). Characterization of Atrophic Changes in the Cerebral Cortex Using Fractal Dimensional Analysis. Brain Imaging and Behavior, 3(2), 154–166. https://doi.org/10.1007/s11682-008-9057-9
15. Kiselev V. G., Hahn K. R., Auer D. P. (2003). Is the brain cortex a fractal? Neuroimage, 20(3), 1765–1774. https://doi.org/10.1016/s1053-8119(03)00380-x
16. Landini G. (2011). Fractals in microscopy. Journal of Microscopy, 241(1), 1–8. https://doi.org/10.1111/j.1365-2818.2010.03454.x
17. Lee J. M., Yoon U., Kim J. J., Kim I. Y., Lee D. S., Kwon J. S., Kim S. I. (2004). Analysis of the hemispheric asymmetry using fractal dimension of a skeletonized cerebral surface. IEEE Transactions on Biomedical Engineering, 51(8), 1494–1498. https://doi.org/10.1109/TBME.2004.831543
18. Li Z., Zhang J., Wang F., Yang Y., Hu J., Li Q., Tian M., Li T., Huang B., Liu H., Zhang T. (2020). Surface-based morphometry study of the brain in benign childhood epilepsy with centrotemporal spikes. Annals of Translational Medicine, 8(18), 1150. https://doi.org/10.21037/atm-20-5845
19. Madan C. R., Kensinger E. A. (2016). Cortical complexity as a measure of age-related brain atrophy. NeuroImage, 134, 617–629. https://doi.org/10.1016/j.neuroimage.2016.04.029
20. Mandelbrot B. B. (1977). Fractals – form, chance and dimension. San Francisco: W.H. Freeman and Company.
21. Mandelbrot B. B. (1982). The fractal geometry of nature. San Francisco: W. H. Freeman and Company.
22. Maryenko N., Stepanenko O. (2023). Atrophic age-related changes in cerebral hemispheres: Euclidean geometry based morphometry of MRI brain scans. Acta Morphologica et Anthropologica, 30(3–4), 40–52. https://doi.org/10.7546/AMA.30.3-4.2023.06
23. Maryenko N., Stepanenko O. (2023). Fractal Dimension of Silhouette Magnetic Resonance Brain Images as a Measure of Age-Associated Changes in Cerebral Hemispheres. Duzce Medical Journal, 25 (1), 27–37. https://doi.org/10.18678/dtfd.1180625

24. Maryenko N., Stepanenko O. (2023). Quantitative characterization of age-related atrophic changes in cerebral hemispheres: A novel "contour smoothing" fractal analysis method. Translational Research in Anatomy, 33, 100263. https://doi.org/10.1016/j.tria.2023.100263
25. Podgórski P., Bladowska J., Sasiadek M., Zimny A. (2021). Novel Volumetric and Surface-Based Magnetic Resonance Indices of the Aging Brain – Does Male and Female Brain Age in the Same Way? Frontiers in Neurology, 12, 645729. https://doi.org/10.3389/fneur.2021.645729
26. Rajagopalan V., Das A., Zhang L., Hillary F., Wylie G. R., Yue G. H. (2019). Fractal dimension brain morphometry: a novel approach to quantify white matter in traumatic brain injury. Brain Imaging and Behavior, 13(4), 914–924. https://doi.org/10.1007/s11682-018-9892-2
27. Riello R., Sabattoli F., Beltramello A., Bonetti M., Bono G., Falini A., Magnani G., Minonzio G., Piovan E., Alaimo G., Ettori M., Galluzzi S., Locatelli E., Noiszewska M., Testa C., Frisoni G. B. (2005). Brain volumes in healthy adults aged 40 years and over: a voxel-based morphometry study. Aging Clinical and Experimental Research, 17(4), 329–336. https://doi.org/10.1007/BF03324618
28. Roura E., Maclair G., Andorrà M., Juanals F., Pulido-Valdeolivas I., Saiz A., Blanco Y., Sepulveda M., Llufriu S., Martínez-Heras E., Solana E., Martinez-Lapiscina E. H.,Villoslada P. (2021). Cortical fractal dimension predicts disability worsening in Multiple Sclerosis patients. NeuroImage Clinical, 30, 102653. https://doi.org/10.1016/j.nicl.2021.102653
29. Schneider C. A., Rasband W. S., Eliceiri K. W. (2012). NIH Image to ImageJ: 25 years of image analysis. Nature Methods, 9(7), 671–675. https://doi.org/10.1038/nmeth.2089
30. Walhovd K. B., Fjell A. M., Reinvang I., Lundervold A., Dale A. M., Eilertsen D. E., Quinn B. T., Salat D., Makris N., Fischl B. (2005). Effects of age on volumes of cortex, white matter and subcortical structures. Neurobiology of Aging, 26(9), 1261–1270; discussion 1275–8. https://doi.org/10.1016/j.neurobiolaging.2005.05.020
31. Zhang L., Dean D., Liu J. Z., Sahgal V., Wang X., Yue G. H. (2007). Quantifying degeneration of white matter in normal aging using fractal dimension. Neurobiology of Aging, 28(10), 1543–1555. https://doi.org/10.1016/j.neurobiolaging.2006.06.020
32. Zhang L., Liu J. Z., Dean D., Sahgal V., Yue G. H. (2006). A three-dimensional fractal analysis method for quantifying white matter structure in human brain. Journal of Neuroscience Methods, 150(2), 242–253. https://doi.org/10.1016/j.jneumeth.2005.06.021
33. Zheng F., Liu Y., Yuan Z., Gao X., He Y., Liu X., Cui D., Qi R., Chen T., Qiu J. (2019). Age-related changes in cortical and subcortical structures of healthy adult brains: A surface-based morphometry study. Journal of Magnetic Resonance Imaging, 49(1), 152–163. https://doi.org/10.1002/jmri.26037

34. Zhuo C., Li G., Chen C., Ji F., Lin X., Jiang D., Tian H., Wang L., Lin X., Ping J. (2020). Left cerebral cortex complexity differences in sporadic healthy individuals with auditory verbal hallucinations: A pilot study. Psychiatry Research, 285, 112834. https://doi.org/10.1016/j.psychres.2020.112834

Address for correspondence:
Nataliia Maryenko
Department of Histology, Cytology and Embryology
Kharkiv National Medical University
4 Nauky Avenue, 61022, Kharkiv, Ukraine
E-mail: maryenko.n@gmail.com, ni.marienko@knmu.edu.ua